Journal of Risk Analysis and Crisis Response, 2026, 16(4), 1-8
https://jracr.com/
ISSN Print: 2210-8491
ISSN Online: 2210-8505

Letter

Integrating machine-learning-based landslide susceptibility and vulnerability for slope-unit risk assessment

Chaolong Kang [1], Haidong Li [2,3,*]

[1] Tibet Geological and Mineral Survey Bureau, No. 2 Geological Team
[2] Faculty of Geosciences and Engineering, Southwest Jiaotong University, Chengdu (611756), China
[3] Yibin Research Institute, Southwest Jiaotong University, Yibin 644000, China
* Correspondence: 19181959646@163.com

Received: ; Received in revised form: ; Accepted: ; Available online:

Abstract: Landslide susceptibility identifies terrain associated with landslide occurrence, whereas risk prioritization also requires information on the vulnerability of threatened elements. This letter presents a slope-unit framework linking machine-learning susceptibility prediction, SHAP-based interpretation, and vulnerability-based relative risk classification. Four models were evaluated using a regional test dataset, and the selected model was applied to 393 slope units. XGBoost achieved the highest area under the receiver operating characteristic curve (AUC = 0.952), followed by random forest (0.904), logistic regression (0.662), and support vector machine (0.600). Paired DeLong tests indicated significant differences between XGBoost and logistic regression (LR) and support vector machine (SVM), but not random forest (RF). SHAP analysis identified slope, relief, and elevation as the leading predictors, accounting for 62.83% of normalized grouped importance. High and very high relative risk occupied 21.34% of the mapped slope-unit area. Of 69 very-high-susceptibility units, only 13 were classified as very high risk after vulnerability integration. The framework supports the identification of priority slope units for targeted field investigation, monitoring, and mitigation planning.

Keywords: Landslide susceptibility; Vulnerability; Risk assessment; Explainable machine learning

1. Introduction

Landslides threaten human lives, settlements, and infrastructure in mountainous regions. Their occurrence reflects interactions among terrain, geological conditions, hydrological processes, and human disturbance, while their consequences also depend on the vulnerability of threatened elements [1-4]. Reliable assessment is therefore needed to identify landslide-prone slopes and provide spatial information for investigation, monitoring, and mitigation planning.

Approaches to landslide assessment have evolved from expert-based classification and statistical analysis to machine-learning prediction [5-8]. Models such as logistic regression, random forest, support vector machine, and gradient boosting provide alternative ways to characterize relationships between conditioning factors and historical landslide occurrence [9-11]. More recently, explainable machine-learning techniques, including SHapley Additive exPlanations (SHAP), have enabled examination of predictor contributions at both individual and aggregate levels [12,13]. Slope units provide a geomorphologically meaningful spatial basis for these analyses and facilitate the integration of environmental and vulnerability information [14,15].

These methodological advances address complementary aspects of assessment, but their connection requires careful consideration. Predictive performance indicates how well a model discriminates recorded landslide occurrence, whereas model interpretation describes how conditioning factors contribute to its predictions. Neither alone provides a complete basis for risk assessment. Vulnerability information must be incorporated through explicit integration rules, with consistent spatial units and clearly defined outputs [16]. A coherent framework is therefore needed to connect prediction, interpretation, and relative risk classification.

We present a slope-unit-based framework linking machine-learning susceptibility modeling, SHAP-based interpretation, and vulnerability assessment. The framework combines regional model evaluation with application-area prediction and integrates susceptibility and vulnerability through a decision matrix. Its implementation illustrates how complementary analytical components can be organized into a transparent assessment workflow to support targeted landslide investigation, monitoring, and mitigation planning.

2. From geohazard identification to risk assessment

2.1 Characterizing landslide susceptibility

Slope units were adopted as the spatial basis for susceptibility modeling and subsequent risk assessment. Units containing historical landslide records were assigned positive labels, while the remaining units were treated as having no recorded landslides. Nine conditioning factors were selected: elevation, slope, relief, aspect, distance to roads, distance to rivers, strata, bedding dip angle class, and slope structure.

Continuous predictors retained their numerical values, while bedding dip angle class was represented as an ordinal variable. Identifiers, vulnerability attributes, and existing zoning results were excluded from model inputs. Pairwise associations among continuous predictors were examined using Spearman correlation analysis. LR, RF, SVM, and XGBoost were compared, with standardization applied where required and class weighting used to address sample imbalance. Hyperparameters were selected within the training subset using five-fold cross-validation with ROC-AUC as the scoring metric. Grid search was used for LR and SVM, while randomized search was used for RF (50 parameter settings) and XGBoost (80 parameter settings); the selected settings were LR (C = 0.01, solver = lbfgs), RF (n estimators = 500, maximum depth = 15, minimum samples per leaf = 5), SVM (C = 100, gamma = scale, RBF kernel), and XGBoost (n estimators = 200, maximum depth = 7, learning rate = 0.01, subsample = 0.8, column subsampling = 1, and minimum child weight = 5). A stratified 70:30 split produced a test subset of 348 units, including 57 positive and 291 negative samples. The 348 units refer to the held-out subset used for model evaluation. Model discrimination was evaluated using ROC-AUC. Two-sided paired DeLong tests compared XGBoost with the other models, with Holm adjustment across the three comparisons [17,18].

The selected model was applied without retraining to the 393 application-area units. Susceptibility scores were classified using the Jenks natural breaks method, with upper class boundaries of 0.080072, 0.197054, 0.378781, 0.671783, and 0.973803, corresponding to very low, low, moderate, high, and very high susceptibility, respectively. SHapley Additive exPlanations (SHAP) were calculated for the application-area units to interpret the selected model [19]. Contributions from one-hot-encoded features belonging to the same factor were summed for each unit before calculating mean absolute SHAP importance. This retained a nine-factor interpretation of the encoded model.

SHAP values were expressed on the log-odds scale, with positive and negative contributions indicating increases and decreases in model output, respectively.

2.2 Representing vulnerability

Population and economic vulnerability were evaluated at the slope-unit scale in accordance with the Specification for Geological Hazard Risk Survey and Assessment (1:50,000) (DZ/T 0438-2023) [20]. Population and economic vulnerability were evaluated separately and combined into a comprehensive classification.

The potentially threatened population was estimated as:

$$C_p = N_p V_p \tag{1}$$

Where N_p is the total population within a slope unit and V_p is the population vulnerability reduction coefficient. The coefficient reflects hazard intensity, mitigation and warning conditions, and the capacity for protection and evacuation.

Potential economic losses were estimated as:

$$C_e = \sum_{j=1}^{n} V_{e,j} N_{e,j} \tag{2}$$

Where $N_{e,j}$ is the economic value of asset category j, estimated from asset quantities and corresponding unit costs, and $V_{e,j}$ is its vulnerability reduction coefficient.

Population and economic vulnerability were classified into four levels using thresholds of 30, 100, and 300 persons and CNY 3, 10, and 30 million, respectively. Comprehensive vulnerability was assigned as the higher of the two component classes:

$$V_i = \max\left[g_{p'}(C_{p,i})\, g_e(C_{e,i})\right] \tag{3}$$

Where g_p and g_e represent the respective classification rules. The resulting low, moderate, high, and very high vulnerability classes were integrated with susceptibility for relative risk assessment.

2.3 Integrating risk components and evaluating the framework

Susceptibility and comprehensive vulnerability were integrated at the slope-unit scale using a decision matrix (Table 1). The decision matrix provides an ordinal rule for combining susceptibility and comprehensive vulnerability. For a given susceptibility class, higher vulnerability can raise the assigned relative risk class, allowing slope units with greater potential consequences to receive higher priority. The resulting classes support relative prioritization rather than representing calibrated loss probabilities. Five susceptibility classes and four vulnerability classes were combined to assign four relative risk levels: low, moderate, high, and very high. For slope unit i, the classification was expressed as:

$$R_i = M(S_i, V_i) \tag{4}$$

Where S_i and V_i denote susceptibility and comprehensive vulnerability classes, respectively, and M represents the matrix-based integration rule. This procedure provides a consistent classification while preserving the separate contributions of susceptibility and vulnerability.

Model performance was assessed using ROC-AUC, and SHAP analysis was used to interpret predictor contributions. The number and area of slope units in each risk class were summarized,

while cross-tabulation showed how vulnerability differentiated risk levels within the same susceptibility class. Figure 1 presents the complete workflow.

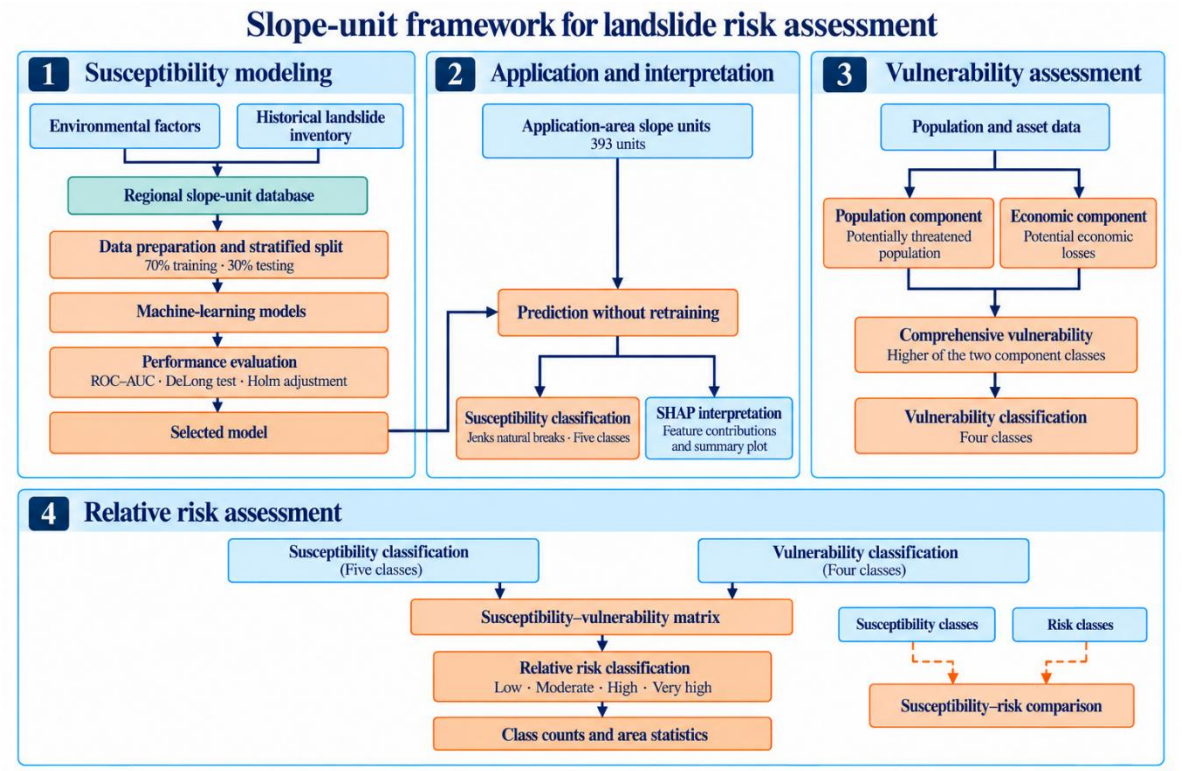


Figure 1. Workflow for slope-unit landslide risk assessment

3. Application and evaluation of the framework

3.1 Case description and implementation

The framework was applied to 393 slope units in northwestern Yunyang County, southwestern China. The area is characterized by dissected mountainous terrain and interbedded sedimentary formations. The 393 units were matched by slope-unit ID to records in the encoded predictor database used for susceptibility model development and were used to generate the application-area maps. They constitute the spatial subset assessed for risk. Previously delineated geohazard zones defined the assessment boundary but were excluded from susceptibility predictors. We organized environmental factors, historical landslide records, and vulnerability information at the slope-unit scale. Susceptibility and comprehensive vulnerability were assessed for the same units and integrated through the decision matrix in Table 1 to produce the relative risk classification.

Table 1. Decision matrix for integrating landslide susceptibility and comprehensive vulnerability into relative risk classes.

Landslide susceptibility	Low vulnerability	Moderate vulnerability	High vulnerability	Very high vulnerability
Very low	Low	Low	Moderate	Moderate
Low	Low	Low	Moderate	Moderate
Moderate	Low	Moderate	High	High
High	Moderate	Moderate	High	Very high
Very high	Moderate	High	Very high	Very high

3.2 Key evaluation findings

XGBoost achieved the highest test AUC of 0.952, followed by RF (0.904), LR (0.662), and SVM (0.600) (Figure 2a). Paired DeLong tests with Holm adjustment indicated significant differences between XGBoost and both LR and SVM (adjusted $p<0.001$). The difference between XGBoost and RF was not statistically significant (adjusted $p=0.113$). XGBoost was retained for susceptibility mapping based on its highest observed AUC.

The SHAP summary plot ranked slope, relief, and elevation as the leading predictors for the 393 application-area units (Figure 2b). Their normalized grouped importance values were 28.88%, 20.22%, and 13.73%, respectively, totaling 62.83%. Higher mean slope values generally contributed negatively to model outputs, whereas lower values more frequently produced positive contributions. Low relief values included pronounced negative contributions, while higher values more often occurred near zero or on the positive side. These patterns reflect the fitted model and should be interpreted in relation to the historical inventory and the use of slope-unit mean values.

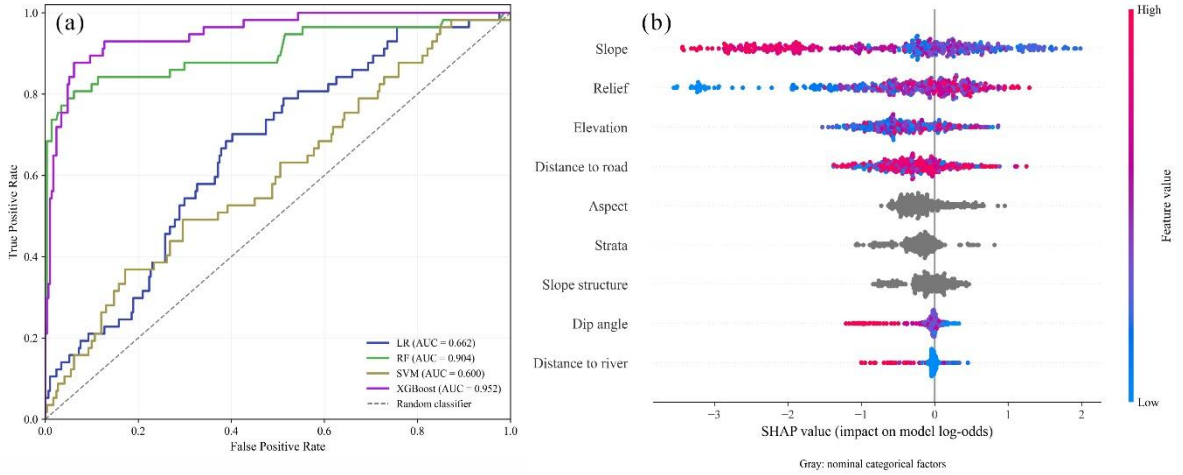


Figure 2. Model evaluation and SHAP analysis. (a) ROC curves for the 348-unit test set. (b) SHAP summary for the selected XGBoost model on the 393 application-area units.

Figure 3 presents the spatial distributions of susceptibility, comprehensive vulnerability, and relative risk. Vulnerability integration differentiated the susceptibility pattern, producing four relative risk classes. Low risk occupied the largest share of the assessed slope-unit area, while high and very high risk occurred in a smaller set of units distributed across the application area. Comparing the susceptibility and relative risk maps shows how vulnerability modifies the susceptibility-based classification and results in four relative risk classes.

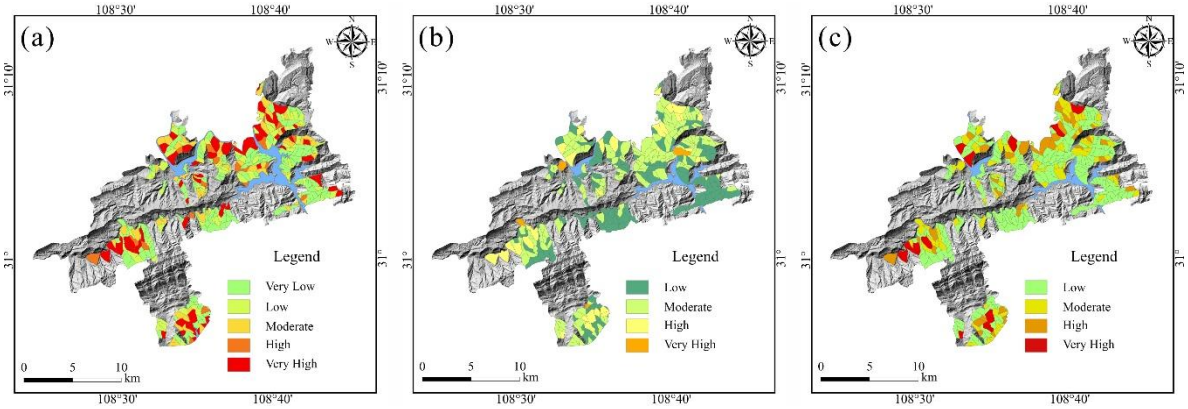


Figure 3. Spatial distributions of (a) landslide susceptibility, (b) comprehensive vulnerability, and (c) relative landslide risk in the application area.

The risk-class statistics are summarized in Table 2. Low risk was the largest class, comprising 261 units (66.41%) and 57.33% of the mapped area. Moderate risk comprised 76 units (19.34%) and 21.32% of the area. High and very high risk comprised 43 and 13 units, respectively, and together covered 21.34% of the area. The locations of these higher-risk units are shown in Figure 3c and provide a focused basis for further investigation and mitigation planning. Cross-tabulation showed how vulnerability differentiated risk within the same susceptibility class. Among the 69 very-high-susceptibility units, 19 were classified as moderate risk, 37 as high risk, and 13 as very high risk. Of the 20 high-susceptibility units, 18 received moderate risk and two high risk. Conversely, 17 units with very low or low susceptibility were assigned moderate risk because of their higher vulnerability. The integrated classification therefore combines information on landslide occurrence potential with population and economic vulnerability to support assessment priorities.

Table 2. Distribution of slope units and mapped area across relative landslide risk classes

Relative risk class	No. of slope units	Slope units (%)	Mapped area (%)
Low	261	66.41	57.33
Moderate	76	19.34	21.32
High	43	10.94	13.23
Very high	13	3.31	8.11
Total	393	100.00	100.00

Note: Percentages may not sum to 100% because of rounding.

4. Limitations and prospects

Several limitations should be considered when applying the proposed framework. Historical inventories may omit past landslides and potentially unstable slopes, while spatial dependence among slope units may affect performance estimates obtained from random data splitting [21]. SHAP explains the fitted model's predictions, but the attribution patterns require interpretation alongside local geological conditions and field observations. Vulnerability estimates introduce additional uncertainty through the use of prescribed reduction coefficients, asset values, and classification thresholds [22,23]. Future work should incorporate updated inventories, spatially independent testing, and locally calibrated vulnerability parameters. Sensitivity analysis of class boundaries and decision-matrix rules would further clarify the stability of identified priority areas.

Overall, this study connects susceptibility prediction, model interpretation, and vulnerability assessment within a common slope-unit framework. The application illustrates how machine-

learning outputs and population and economic vulnerability can be combined to produce interpretable relative risk classifications. With further field validation and improved representation of landslide intensity and consequences, the framework could support targeted slope investigation, monitoring, and mitigation planning.

Contributions: C. K. designed the research and wrote the manuscript. H. L. processed the data and wrote the manuscript. All authors reviewed the manuscript.

Funding: This research was funded by Yibin City Science and Technology program (25KJJH0101, 2024MZ001, YBSCXY2023020006, YBSCXY2023020007).

Conflicts of Interest: The authors declare no conflicts of interest.

References

[1] Hong, B., Shao, B., Wang, B., Zhao, J., Qian, J., Guo, J., Xu, Y., Li, C., & Zhu, B. (2023). Using the meteorological early warning model to improve the prediction accuracy of water damage geological disasters around pipelines in mountainous areas. Science of The Total Environment, 889, 164334. https://doi.org/10.1016/j.scitotenv.2023.164334

[2] Shen, Y., Guo, Q., Liu, Z., Shen, Y., Jia, Y., & Wei, Y. (2025). Prediction of drought-flood prone zones in inland mountainous regions under climate change with assessment and enhancement strategies for disaster resilience in high-standard farmland. Agricultural Water Management, 309, 109349. https://doi.org/10.1016/j.agwat.2025.109349

[3] Huang, F., Yang, Y., Ma, G., Rezania, M., Chang, Z., Catani, F., Jiang, B., Chen, X., & Guo, F. (2026). Real-time early warning of landslide disaster risks on major highways in Ganzhou City, China. Journal of Rock Mechanics and Geotechnical Engineering. https://doi.org/10.1016/j.jrmge.2025.10.023

[4] Yin, X., Gao, F., Daniel, C., Yu, H., Wongbae, L. Z., Li, P., Pan, Y., Liu, H., & Liu, Q. (2025). Toward disaster management in rock engineering: Automated machine learning paradigm for predicting the uniaxial compressive strength of rock materials. Geohazard Mechanics, 3(4), 249-260. https://doi.org/10.1016/j.ghm.2025.11.006

[5] Zhang, Y., Yao, R., Cicchella, D., Luo, M., & Galal Uddin, M. (2026). Decoupling geogenic and anthropogenic drivers of groundwater natural background levels using machine learning and high-resolution maps. Journal of Hydrology, 678, 136053. https://doi.org/10.1016/j.jhydrol.2026.136053

[6] Joshi, B. R., Bhandary, N. P., Acharya, I. P., Niraj, K. C., & Bhandari, C. (2026). Integration of information value with machine learning method for an enhanced predictive performance in landslide susceptibility mapping. Discover Geoscience, 4(1), 152. https://doi.org/10.1007/s44288-026-00517-2

[7] Jia, J., & Ye, W. (2023). Deep Learning for Earthquake Disaster Assessment: Objects, Data, Models, Stages, Challenges, and Opportunities. Remote Sensing, 15(16), 4098. https://doi.org/10.3390/rs15164098

[8] Saha, S., Barman, A., Saha, A., Hembram, T. K., Pradhan, B., & Alamri, A. (2024). Deep learning algorithms based landslide vulnerability modeling in highly landslide prone areas of Tamil Nadu, India. Geosciences Journal, 28(6), 1013-1038. https://doi.org/10.1007/s12303-024-0044-y

[9] Li, H., Wang, Y., Wu, Y., Wang, J., Shi, K., Luo, L., Zuo, L., & Zhang, Y. (2026). Harnessing machine learning and multi-source data fusion for regional geohazard risk assessment of a rapidly urbanizing mountainous region. Scientific Reports. https://doi.org/10.1038/s41598-026-70394-9

[10] Chen, W., Pourghasemi, H. R., Kornejady, A., & Zhang, N. (2017). Landslide spatial modeling: Introducing new ensembles of ANN, MaxEnt, and SVM machine learning techniques. Geoderma, 305, 314-327. https://doi.org/10.1016/j.geoderma.2017.06.020

[11] Liu, Y., Xu, Y., Huang, J., Liu, H., Fang, Y., & Yu, Y. (2024). A comparative study of intelligent prediction models for landslide susceptibility: random forest and support vector machine [Original Research]. Frontiers in Earth Science, Volume 12 - 2024. https://doi.org/10.3389/feart.2024.1519771

[12] Ullah, Y., Shafique, M., Yu, L., & Shah, N. A. (2024). Landslides hazard, vulnerability and risk mapping in the data-poor region of northern Pakistan. Environmental Earth Sciences, 83(19), 560. https://doi.org/10.1007/s12665-024-11858-x

[13] Saha, A., Villuri, V. G. K., & Bhardwaj, A. (2025). Development and assessment of a novel hybrid machine learning-based landslide susceptibility mapping model in the Darjeeling Himalayas. Stochastic Environmental Research and Risk Assessment, 39(10), 4145-4168. https://doi.org/10.1007/s00477-023-02528-8

[14] Zhou, Y., Xue, L., Ding, H., Wang, H., Huang, K., Li, L., & Li, Z. (2025). Landslide Risk Assessment as a Reference for Disaster Prevention and Mitigation: A Case Study of the Renhe District, Panzhihua City, China. Remote Sensing, 17(13), 2120. https://doi.org/10.3390/rs17132120

[15] Tran, T. X., Liu, S., Ha, H., Bui, Q. D., Nguyen, L. Q., Nguyen, D. Q., Trinh, C.-T., & Luu, C. (2024). A Spatial Landslide Risk Assessment Based on Hazard, Vulnerability, Exposure, and Adaptive Capacity. Sustainability, 16(21), 9574. https://doi.org/10.3390/su16219574

[16] Mavrouli, O., Fotopoulou, S., Pitilakis, K., Zuccaro, G., Corominas, J., Santo, A., Cacace, F., De Gregorio, D., Di Crescenzo, G., Foerster, E., & Ulrich, T. (2014). Vulnerability assessment for reinforced concrete buildings exposed to landslides. Bulletin of Engineering Geology and the Environment, 73(2), 265-289. https://doi.org/10.1007/s10064-014-0573-0

[17] Yin, X., Liu, B., Chen, P., Lin, Y., Li, Z., & Fu, D. (2026). Multisource Remote Sensing Assessment of Ocean Responses and Rainfall-Related Flood Hazards During Severe Tropical Storm Maysak. Remote Sensing, 18(21), 3729. https://doi.org/10.3390/rs18213729

[18] Delong, E. R., Delong, D. M., & Clarke-Pearson, D. L. (1988). Comparing the areas under two or more correlated receiver operating characteristic curves: a nonparametric approach. Biometrics, 44(3), 837. https://doi.org/10.2307/2531595.

[19] Wang, Y., Wang, W., Fan, X., Wang, X., & Chen, L. (2026). Assessing the Added Value of InSAR Deformation Features for Landslide Susceptibility Mapping Using Spatial Validation and SHAP. Remote Sensing, 18(21), 3726. https://doi.org/10.3390/rs18213726

[20] Ministry of Natural Resources of the People's Republic of China. (2023). Specification for Geological Hazard Risk Survey and Assessment (1:50,000) [in Chinese] (DZ/T 0438-2023).

[21] Liu, D., Cheng, W., Qian, Z., Deng, J., Liu, J., & Wang, X. (2023). Boundary Delineator for Martian Crater Instances with Geographic Information and Deep Learning. Remote Sensing, 15(16), 4036. https://doi.org/10.3390/rs15164036

[22] Peng, M., Wang, Y., Ma, C., Wang, H., Meng, S., Shi, Z., Chu, W., & Xu, J. (2025). Landslide susceptibility assessment integrating deep transfer learning and physical models in the Baihetan reservoir area, China. Journal of Rock Mechanics and Geotechnical Engineering. https://doi.org/10.1016/j.jrmge.2025.07.007

[23] He, Y., Ding, M., Duan, Y., Zheng, H., Wu, J., & Feng, L. (2025). Exploring the dynamic impact of urbanization on landslide susceptibility in Sichuan Province using an explainable XGBoost model. Engineering Geology, 357, 108372. https://doi.org/10.1016/j.enggeo.2025.108372



Copyright © 2026 by the authors. This is an open access article distributed under the CC BY-NC 4.0 license (http://creativecommons.org/licenses/by-nc/4.0/).